ACS Energy Letters

http://pubs.acs.org/journal/aelccp

Lithium Metal Batteries Enabled by Synergetic Additives in Commercial Carbonate Electrolytes

Nan Piao,[▽] Sufu Liu,[▽] Bao Zhang,[▽] Xiao Ji, Xiulin Fan, Li Wang, Peng-Fei Wang, Ting Jin, Sz-Chian Liou, Huicong Yang, Jianjun Jiang, Kang Xu, Marshall A. Schroeder, Xiangming He,* and Chunsheng Wang*

Cite This: *ACS Energy Lett.* 2021, 6, 1839−1848

Read Online

ACCESS | Metrics & More | Article Recommendations | Supporting Information

ABSTRACT: The lithium metal anode is considered as the ultimate choice for high-energy-density batteries. However, the organic-dominated solid electrolyte interphase (SEI) formed in carbonate electrolytes has a low interface energy against metallic Li as well as a high resistance, resulting in a low Li plating/stripping Coulombic efficiency (CE) of less than 99.0% and severe Li dendrite growth. Herein, inorganic-enhanced LiF-Li_3N SEI is designed in commercial 1 M $LiPF_6$/EC-DMC electrolytes by introducing lithium nitrate ($LiNO_3$) and fluoroethylene carbonate (FEC) through a small amount of sulfolane (SL) as a carrier solvent owing to the high solubility of SL for both carbonate solvents and $LiNO_3$. The comprehensive characterizations and simulations demonstrate that the synergistic interaction of $LiNO_3$ and FEC additives alters the solvation structure of 1 M $LiPF_6$/EC-DMC electrolytes and forms additive-derived LiF-Li_3N SEI, which increases the average Li CE up to 99.6% in 100 cycles. The designed carbonate electrolyte enables the Li/$LiNi_{0.80}Co_{0.15}Al_{0.05}O_2$ (NCA) cell with a lean lithium metal anode (∼50 μm) to achieve an average CE of 99.7% and a high capacity retention of 90.8% after 150 cycles. This work offers a simple and economical strategy to realize high-performance lithium metal batteries in commercial carbonate electrolytes.

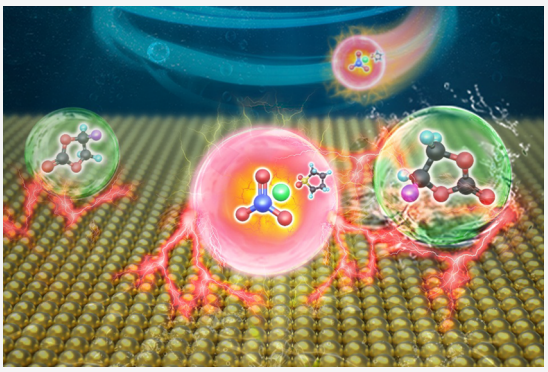

Lithium ion batteries (LIBs) are approaching the energy density limit and lagging behind the need for electric vehicles and energy storage systems.[1,2] Benefiting from the highest theoretical specific capacity (3860 mAh g^{-1}) and lowest electrochemical potential (−3.04 V vs standard hydrogen electrode), the lithium metal anode has attracted wide attention to further improve the energy density of LIBs.[3−6] However, the lithium anode in commercial carbonate electrolytes faces challenges of lithium dendrite growth and low Coulombic efficiency (CE), because the organic−inorganic solid electrolyte interphase (SEI) formed in carbonate electrolytes is highly lithiophilic to metallic Li. The strong bonding between SEI and Li forces a similar volume change of SEI as Li, resulting in cracks of SEI. Further, the low interface energy of SEI to metallic Li promotes dendrite growth through cracked SEI.[7] Hence, a lithiophobic SEI with a high interfacial energy to Li is highly desirable to resist the volume deformation. Recently, extensive efforts on regulating SEI components have been conducted by tuning electrolyte composition[8−13] and constructing artificial SEI.[14−16] Among them, the electrolyte additive strategy has been considered as the most effective and economical strategy.[17,18]

Fluoroethylene carbonate (FEC) has been regarded as one of the most effective components to enhance the stability of lithium metal anodes when it is used as the cosolvent or the additive in carbonate electrolytes. FEC has a lower unoccupied molecular orbital (LUMO) than carbonate solvents, as well as excellent miscibility for most solvents and lithium salts, which can be preferentially reduced compared with carbonate solvents.[19,20] FEC contributes to form more inorganic LiF component in the inner SEI, which has a high interfacial

Received: February 17, 2021
Accepted: April 2, 2021

Downloaded via UNIV OF MARYLAND COLG PARK on April 22, 2021 at 17:35:50 (UTC).
See https://pubs.acs.org/sharingguidelines for options on how to legitimately share published articles.

© XXXX American Chemical Society

https://doi.org/10.1021/acsenergylett.1c00365
ACS Energy Lett. 2021, 6, 1839−1848

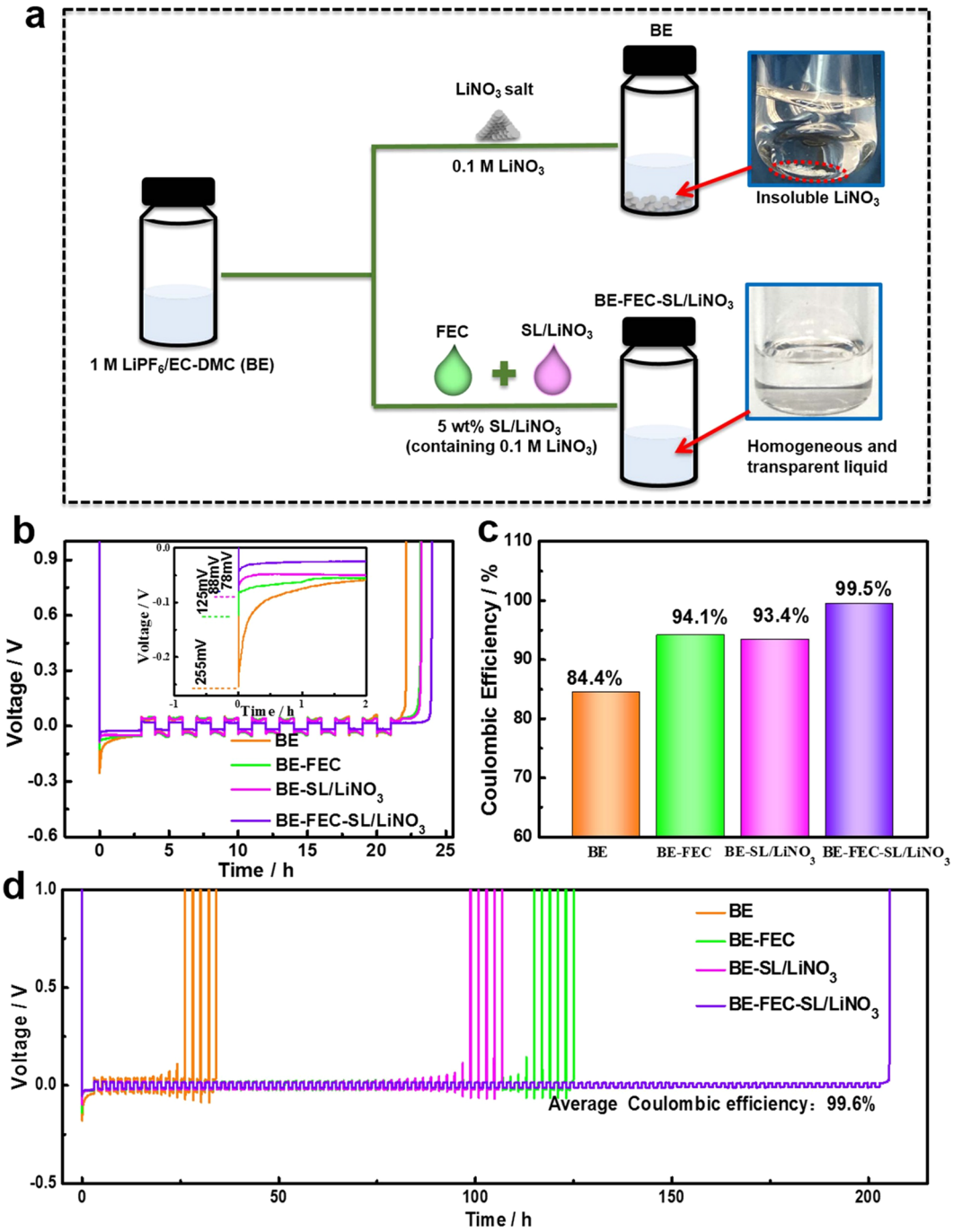

Figure 1. (a) Dissolution of $LiNO_3$ salt in commercial carbonate electrolytes with and without sulfolane (SL) carrier solvent. Adding 5 wt % of 2.2 M SL/$LiNO_3$ solution in 1 M $LiPF_6$/EC-DMC (BE) is equal to introducing 0.1 M $LiNO_3$. (b) Li plating/stripping profiles and (c) Coulombic efficiencies (CE) in BE, BE-FEC, BE-SL/$LiNO_3$, and BE-FEC-SL/$LiNO_3$ at 0.5 mA cm^{-2} and 0.5 mAh cm^{-2}. (d) Li plating/stripping profiles in BE, BE-FEC, BE-SL/$LiNO_3$, and BE-FEC-SL/$LiNO_3$ at 0.5 mA cm^{-2} and 0.5 mAh cm^{-2} for 100 cycles.

energy with metallic Li to inhibit dendrite growth.[21] Meanwhile, the polymeric species formed in the outer layer of FEC-induced SEI maintains good mechanical properties of SEI to resist volume expansion.[17,22] On the other hand, lithium nitrate ($LiNO_3$) has been utilized in ether-based electrolytes of Li/S batteries as a functional additive to stabilize lithium metal anodes.[23,24] It has been confirmed that $LiNO_3$ can effectively adjust the solvation structure of electrolytes and form a nitride-containing SEI on the surface of lithium metal.[24−26] However, ether solvents have poor antioxidation ability, which greatly restricts its application in high-voltage batteries (≥4.3 V).[27] Therefore, introducing $LiNO_3$ into carbonate electrolytes appears to be a more practical and cost-effective method for promoting the high-voltage lithium metal batteries (LMBs). Unfortunately, $LiNO_3$ is less soluble in carbonate electrolytes ($<10^{-5}$ g mL^{-1}),[28] which limits its application in conventional $LiPF_6$/carbonate electrolytes. Recently, several strategies have been reported to overcome the low solubility challenge of $LiNO_3$ in carbonate electrolytes.[28−30] One of the methods is to fill solid $LiNO_3$ powders into the separator or the intermediate layer as a $LiNO_3$ reservoir, which continuously supplies $LiNO_3$ into the electrolyte during its consumption in battery

https://doi.org/10.1021/acsenergylett.1c00365
ACS Energy Lett. 2021, 6, 1839−1848

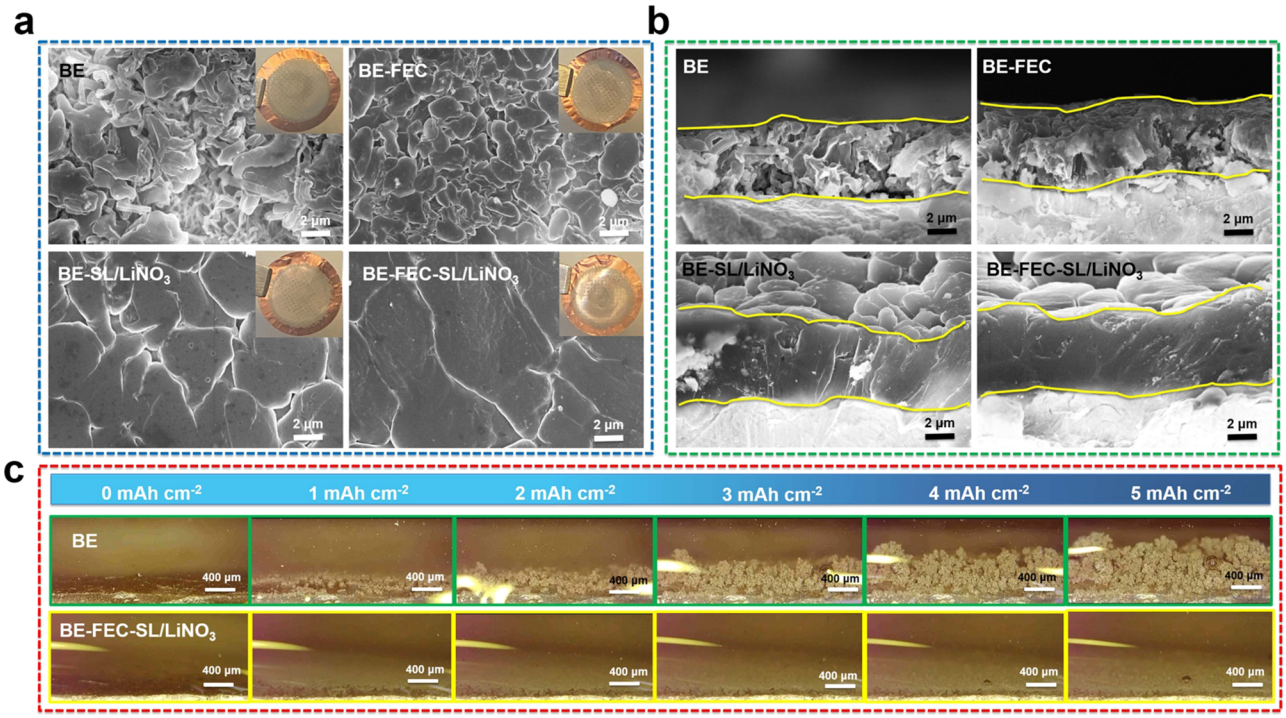

Figure 2. SEM images of the electrodeposited Li at 0.5 and 0.5 mAh cm^{-2} on Cu foils from top view (a) and cross-sectional view (b) in BE, BE-FEC, BE-SL/$LiNO_3$, and BE-FEC-SL/$LiNO_3$. Optical morphology images are inserted in the right corner of (a). (c) In-situ optical microscopy observations of Li deposition process in BE and BE-FEC-SL/$LiNO_3$ to 5 mAh cm^{-2}.

cycling.[28,29] Another method is to introduce $LiNO_3$ into electrolytes using carrier salts (CuF_2,[30] $Sn(OTf)_2$[31]) or solvents (TPFPB or TPFPP)[32] that can dissolve both $LiNO_3$ and electrolytes. However, all these reports still below the fulfilling mark, as evidenced by a low Li plating/stripping CEs of <99.0% in these electrolytes.

Here, we demonstrate for the first time that superior cycling stability with a high CE of the lithium metal anode can be achieved in commercial carbonate electrolytes by introducing a FEC-SL/$LiNO_3$ composite additive, which outperforms the performance in carbonate electrolytes without additive and that with individual FEC or $LiNO_3$ additive. Notably, $LiNO_3$ was introduced into the electrolyte by using a concentrated $LiNO_3$/sulfolane (SL) solution, where the SL carrier solvent has higher $LiNO_3$ solubility and higher oxidation stability than carbonate solvents. As a result, the CE of Li plating/stripping is significantly improved from 84.4% in the baseline 1 M $LiPF_6$/EC-DMC (1:1 by vol) electrolyte (abbreviated as BE) to 99.5% in the BE with FEC-SL/$LiNO_3$ additives (abbreviated as BE-FEC-SL/$LiNO_3$). Due to the synergetic effect of $LiNO_3$ and FEC, a lithiophobic LiF-Li_3N enhanced SEI with high Li-ion conductivity was successfully constructed on the surface of the lithium metal anode, which can reduce the Li nucleation overpotential and suppress Li dendrite growth simultaneously. Moreover, the BE-FEC-SL/$LiNO_3$ electrolyte enables a 4.3 V $LiNi_{0.80}Co_{0.15}Al_{0.05}O_2$ (NCA)/Li (50 μm) full cell to achieve an outstanding capacity retention of 90.8% after 150 cycles with an average CE of 99.7%. This work provides a simple and economic strategy to realize high-voltage LMBs with a supreme performance in commercial carbonate electrolytes.

Li Plating/Stripping in 1 M $LiPF_6$−0.1 M $LiNO_3$/EC-DMC-FEC-SL Electrolytes. The solubility of $LiNO_3$ in commercial carbonate electrolytes is very low (<10^{-5} g mL^{-1}),[28] as demonstrated by the insoluble $LiNO_3$ particles after adding 0.1 M (7 mg mL^{-1}) $LiNO_3$ salt in BE (Figure 1a). However, the highly polar aprotic sulfolane (SL) solvent with a wide voltage window (>5 V vs Li^+/Li) possesses high solubility for both $LiNO_3$ (>2 M) and carbonate electrolytes;[33] thus it can be used as a carrier solvent in carbonate electrolytes to dissolve $LiNO_3$ without compromising the oxidative stability. Since FEC promotes to form LiF in the SEI, both FEC and $LiNO_3$ are selected as additives for commercial carbonate electrolytes using SL as the carrier solvent. As shown in Figure 1a, the obtained BE-FEC-SL/$LiNO_3$ electrolyte maintains a clear and transparent state without sediment. Although adding SL into carbonate electrolytes slightly reduces the Li plating/stripping CE (Figure S1a), the CE can be improved by increasing the salt concentration in SL-based electrolytes.[33,34] To optimize the additive composition, SL/$LiNO_3$ additives with different $LiNO_3$ concentrations were separately added into BE-FEC electrolytes at a fixed amount (5% of BE). As shown in Figure S1b, the CE at 0.5 mA cm^{-2} and 0.5 mAh cm^{-2} significantly increases from 98.3% to 99.5%, when the $LiNO_3$ salt concentration in SL/$LiNO_3$ increases from 0.5 to 2.2 M (saturated state). The SL/$LiNO_3$ (2.2 M) additive has the least free SL solvent and the most $LiNO_3$ content, thereby reducing the impact of SL and promoting the formation of anion-derived inorganic SEI. The addition of 5% SL/$LiNO_3$ (2.2 M) into the carbonate electrolyte is equivalent to introducing 0.1 M $LiNO_3$, which is much higher than the solubility of $LiNO_3$ in carbonate electrolytes.[28] In addition to $LiNO_3$, FEC can also enhance the Li CE. The impact of individual additives (FEC and SL/$LiNO_3$) and their synergetic additive (FEC-SL/$LiNO_3$) on Li CE in BE were further investigated. Panels b and c of Figure 1 display the Li plating/stripping profiles and average CE values in BE with different additives. The CEs in BE, BE-5% FEC, and BE-5% SL/$LiNO_3$ are 84.4%, 94.1%, and 93.4%, respectively. Although FEC or

https://doi.org/10.1021/acsenergylett.1c00365
ACS Energy Lett. 2021, 6, 1839−1848

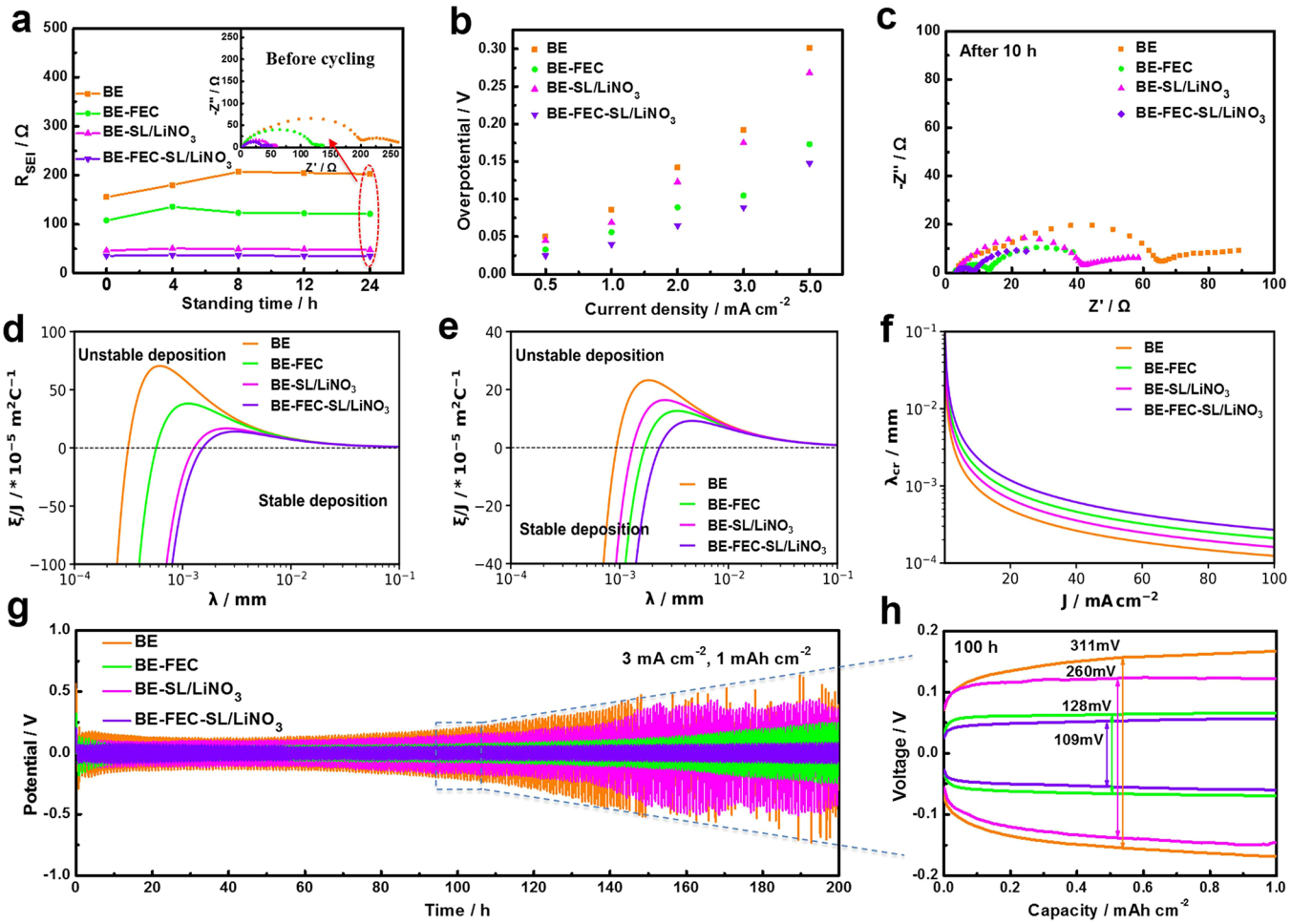

Figure 3. (a) SEI impedance evolution of Li||Li symmetric cells as a function of electrolyte immersion time in various electrolytes (inset with the Nyquist plots after standing for 24 h). (b) Overpotentials of Li||Li symmetric cells in various electrolytes at 1 mAh cm^{-2} with current densities of 0.5−5 mA cm^{-2}. (c) Nyquist plots of the Li||Li symmetric cells after cycling for 10 h at 0.5 mA cm^{-2} and 1 mAh cm^{-2}. (d, e) Current density-scaled growth rate ξ/J of a Li dendrite nucleate size λ at the initial state (d) and the state after cycling for 10 h (e) in various electrolytes. (f) Critical deposit size λ_{cr} ($\xi/J = 0$) of four electrolytes. (g) Galvanostatic cycling performance of Li||Li symmetric cells and (h) its polarization profiles for Li plating/stripping at 100 h in various electrolytes at 3 mA cm^{-2} and 1 mAh cm^{-2}.

$LiNO_3$-containing electrolyte can improve the average CE in BE by nearly 10%, the value is still less than 95% and far below the required value (>99%) for lithium metal anodes, which is consistent with previous results.[19,28,29] However, when 5% FEC and 5% SL/$LiNO_3$ are added together into BE, the synergetic interaction of two additives dramatically improves the average CE up to 99.5%, which is almost 15% higher than that of traditional carbonate electrolytes. The adding amount of FEC and SL/$LiNO_3$ was optimized according to the Li plating/stripping CE test, which shown in Figure S1c. It can be found that the CE in BE-5% FEC-5% SL/$LiNO_3$ has the highest CE among BE-x% FEC-y% SL/$LiNO_3$ ($x + y \leq 10$). Further increasing the additive amount to above 10% in total will cause the salt to precipitate. Therefore, BE-5% FEC-5% SL/$LiNO_3$ is the optimized formulation, which is abbreviated as BE-FEC-SL/$LiNO_3$ in this article unless otherwise specified. The detailed composition, viscosity, and conductivity of the BE, BE-FEC, BE-SL/$LiNO_3$, and BE-FEC-SL/$LiNO_3$ are listed in Table S1. The nucleation onset potential for Li plating in BE-FEC-SL/$LiNO_3$ (78 mV) is also reduced when compared with the ones in BE-SL/$LiNO_3$ (88 mV), BE-FEC (125 mV), and BE (255 mV) (inset in Figure 1b). This is because the additives in BE-FEC-SL/$LiNO_3$ changed the solvation sheath and SEI, resulting in the fastest charge transfer kinetics.[29]

For the long-term Li plating/stripping cycling, a serious voltage fluctuation appears after only 10 cycles in BE due to the low CE. It can be seen from Figure 1d that although the cycling performance of Li plating/stripping in BE-FEC and BE-SL/$LiNO_3$ electrolytes has been greatly improved compared with BE, it still cannot reach 100 cycles due to insufficient CEs. While BE-FEC-SL/$LiNO_3$ delivered stable Li plating/stripping behavior along 100 cycles and the average CE is measured as high as 99.6%. Besides, the average CE in BE-FEC-SL/$LiNO_3$ maintains as high as 99.3% at 1.0 mA cm^{-2} and 1.0 mAh cm^{-2} (Figure S2). The Li plating/stripping CE reported here is one of the best performances for lithium metal anodes in carbonate electrolytes at a low salt concentration (Table S2). In addition, compared with high concentration electrolytes and all-fluorinated electrolytes, BE-FEC-SL/$LiNO_3$ has a comparable CE,[35,36] as well as an obvious cost advantage (Figure S3).

The top and cross-sectional view of scanning electron microscopy (SEM) images for the electrodeposited Li in BE, BE-FEC, BE-SL/$LiNO_3$, and BE-FEC-SL/$LiNO_3$ at 0.5 mA cm^{-2} and 0.5 mAh cm^{-2} are presented in Figure 2a,b. Dendritic and mossy Li deposition were formed in BE. In

https://doi.org/10.1021/acsenergylett.1c00365
ACS Energy Lett. 2021, 6, 1839−1848

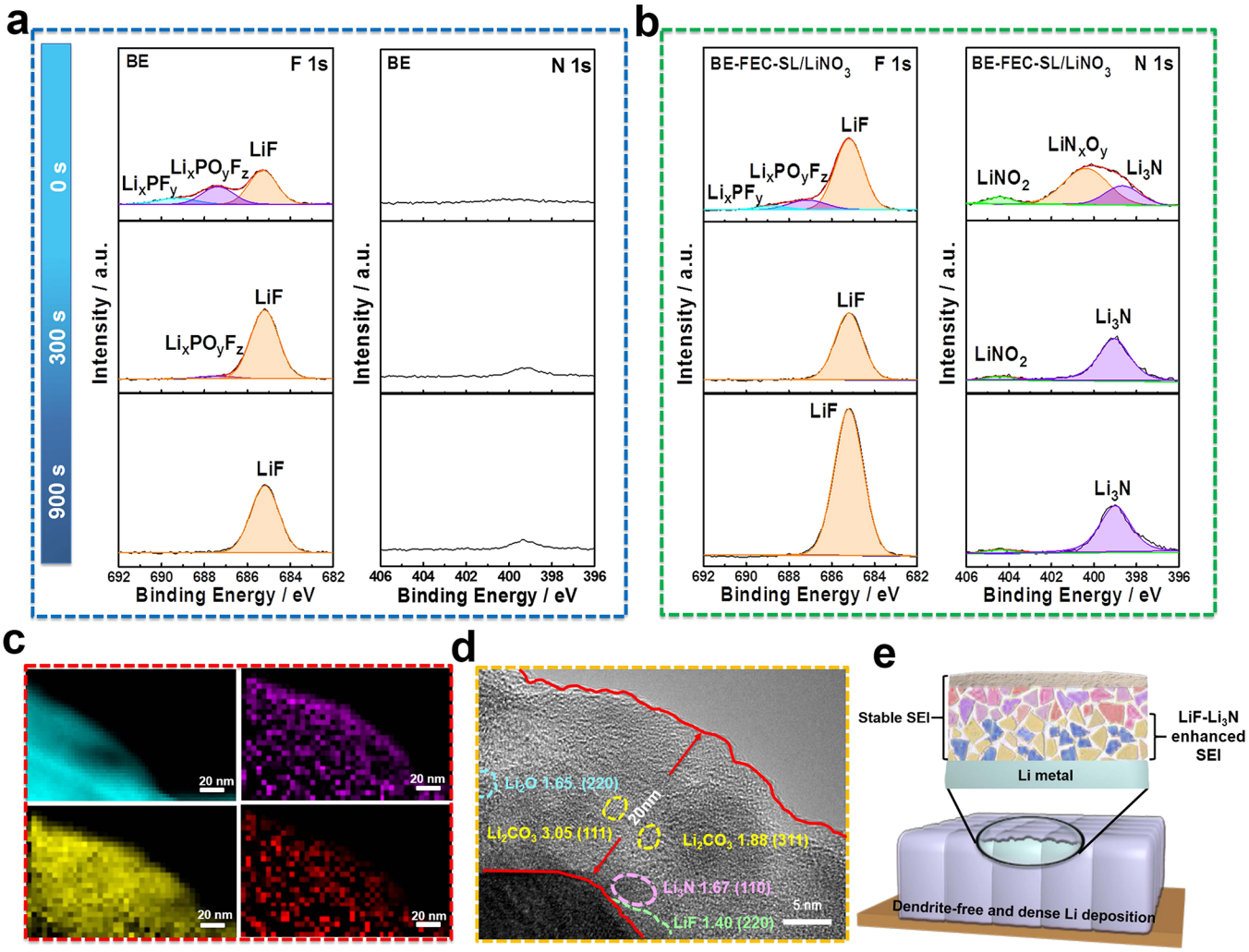

Figure 4. XPS F 1s, N 1s spectra of SEI on lithium metal in BE (a) and BE-FEC-SL/$LiNO_3$ (b). (c) Elemental k-edge mapping of Li, F, N, and O performed by STEM-EELS spectrum imaging. (d) HRTEM image of the SEI formed in BE-FEC-SL/$LiNO_3$. (e) Schematic diagram of the SEI formed in BE-FEC-SL/$LiNO_3$.

contrast, a dendrite-free and compact lithium metal morphology was obtained in the BE-FEC-SL/$LiNO_3$, which is denser than that in BE-FEC and BE-SL/$LiNO_3$. Optical images of the deposited lithium in various electrolytes are also displayed in Figure 2a. The lithium metal deposited in BE appears black and dull with an uneven morphology. Besides, the morphology improvement by individual FEC or SL/$LiNO_3$ additive is not obvious. In contrast, the lithium metal deposited in BE-FEC-SL/$LiNO_3$ still flashes silvery luster with uniform shape, which reveals a less corrosion from the electrolyte due to the protection of a more stable SEI on the lithium metal. In addition, the morphology changes of lithium anodes during Li plating at different capacity in BE (Video S1) and BE-FEC-SL/$LiNO_3$ (Video S2) were in situ monitored using an optical microscope. As shown in Figure 2c, obvious dendrite nucleation and growth can be observed in BE at 1 mAh cm^{-2}. As the deposition capacity increases, the deposited Li becomes looser with a more porous structure, and the tip lithium fragments even break away from the substrate to form "dead lithium" (Figure S4, captured from Video S1), which is consistent with the low CE (84.4%) in BE. In contrast, the morphology of the deposited Li in BE-FEC-SL/$LiNO_3$ is much denser with a smooth morphology. Even at a high plating capacity of 5 mAh cm^{-2}, no clear Li dendrite growth is observed. Therefore, BE-FEC-SL/$LiNO_3$ can effectively decrease the interphase area and suppress Li dendrite growth, resulting in an ultrahigh CE of 99.6%.

The impedance evolution of symmetric Li||Li cells was studied by the electrochemical impedance spectroscopy (EIS), and the semicircle at a high frequency can be attributed to the SEI resistance of lithium metal (R_{SEI}).[37] The R_{SEI} values in different electrolytes were compared as a function of immersion time in Figure 3a, and the specific EIS results are shown in Figure S5. It can be seen that the initial R_{SEI} in BE has the highest value around 156 Ω and gradually grows to 203 Ω after 24 h (inset in Figure 3a). Although the FEC additive helps to reduce R_{SEI}, it still reaches a high value around 121 Ω after the same rest. In contrast, the $LiNO_3$ additive has greatly reduced the interphase impedance, as revealed by the lower resistance in BE-SL/$LiNO_3$ (48 Ω) and the lowest resistance in BE-FEC-SL/$LiNO_3$ (35 Ω). This is mainly because nitrate is more likely to decompose into Li_3N and LiN_xO_y compounds on the surface of lithium metal anode, which are regarded as excellent Li ionic conductors and thus help to enhance the Li ionic transport property of SEI.

https://doi.org/10.1021/acsenergylett.1c00365
ACS Energy Lett. 2021, 6, 1839−1848

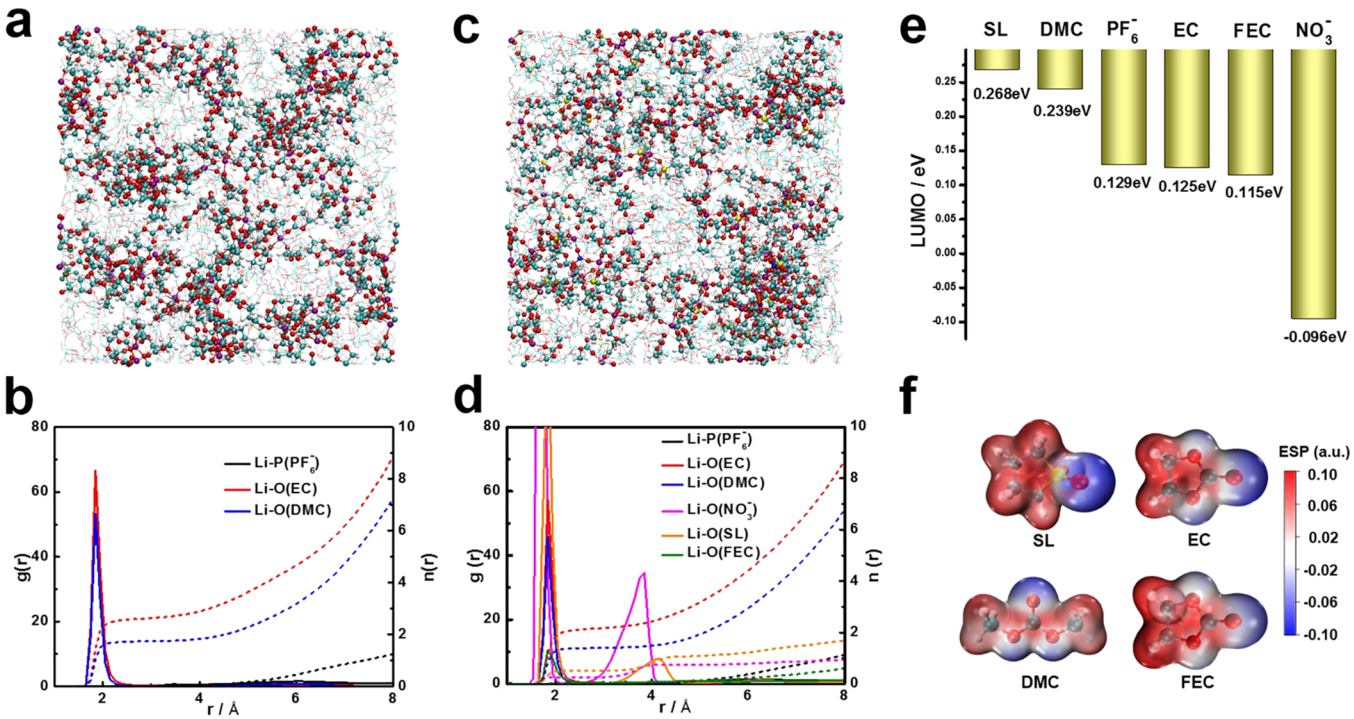

Figure 5. Snapshots of BE (a) and BE-FEC-SL/$LiNO_3$ (c) obtained by MD simulation at 298 K. The Li^+ and their primary coordinated shells (within 2.75 Å of Li^+ ions) are presented by ball and stick models, while the wireframes stand for free solvents. Calculated radial distribution functions ($g(r)$, solid lines) and coordination numbers ($n(r)$), dash lines) for BE (b) and BE-FEC-SL/$LiNO_3$ (d). (e) Calculated lowest unoccupied molecular orbital (LUMO) of different components in BE-FEC-SL/$LiNO_3$. (f) Electrostatic potential (ESP) of SL, EC, DMC, and FEC molecules.

SEI stability was further demonstrated by galvanostatic cycling in the symmetric Li||Li cells under 1 mAh cm^{-2} with various current densities (Figure S6). Generally, FEC contributes to building a compact and mechanically stable SEI composed of the LiF-enhanced thin inner layer and polymeric outer layer, thus reducing the overpotential during Li cycling in Li||Li cells, especially at larger current densities (Figure 3b). LiF not only has low electronic conductivity but also high interfacial energy against Li, thus greatly restraining dendrite growth and improving SEI stability. As shown in Figure 3c, the R_{SEI} of FEC-containing electrolyte is also smaller than $LiNO_3$-containing electrolyte.

Five variables are considered to determine the Li deposition stability of Li anode according to the previous framework,[38] which are Li^+ transference number (t_{Li^+}), ionic conductivity (σ), surface tension (S), current density (J), and shear modulus of separator (G). The current density-scaled growth rate ξ/J of a Li dendrite nucleate size λ and the critical deposit size λ_{cr} of a current density J are shown in Figure 3d−f. At the initial state, R_{SEI} determines Li deposition stability in these four different electrolytes. The additives can decrease R_{SEI} and increase Li deposition stability, especially the $LiNO_3$ additive. After cycling for 10 h, produced SEI films are crucial for Li deposition stability, which can enhance the Li transport at the interface and suppress Li penetration. The additive-derived SEI in BE-FEC-SL/$LiNO_3$ combines high ionic conductivity and high interfacial energy against Li, which greatly suppresses the Li dendrite formation and exhibits the highest Li deposition stability in four electrolytes.

Long-term cycling of Li||Li cells in different electrolytes was also performed at a high current density of 3 mA cm^{-2} and a capacity of 1 mAh cm^{-2}. As exhibited in Figure 3g, the BE shows a distinctly increasing overpotential along with operation time until a huge voltage fluctuation happens after 150 h. It can be found that $LiNO_3$ and FEC are beneficial for improving lithium metal performance, as revealed by the lower overpotentials in BE-SL/$LiNO_3$ (260 mV) and BE-FEC (128 mV) compared with BE (311 mV) after 100 h of cycling (Figure 3h). However, the upward overpotential trend at the later stage in these electrolytes indicates that the individual SL/$LiNO_3$ or FEC additive is not sufficient enough for maintaining the long-term stability, whereas BE-FEC-SL/$LiNO_3$ delivered a steady Li plating/stripping performance in the whole 200 h cycling at 3 mA cm^{-2} and 1 mAh cm^{-2}, as well as the lowest overpotential of 109 mV at 100 h. Besides, BE-FEC-SL/$LiNO_3$ also displayed a stable cycling at 0.5 mA cm^{-2} and 0.5 mAh cm^{-2} for more than 700 h with a minimal variation in the overpotential (Figure S7), which further confirms the synergistic effect of FEC-SL and $LiNO_3$ additives for improving lithium metal performance.

Characterizations of LiF-Li_3N-Enhanced SEI. The SEI compositions formed in BE and BE-FEC-SL/$LiNO_3$ were probed using X-ray photoelectron spectroscopy (XPS) (Figure 4a,b, Figures S7−S9). As shown in F 1s spectra from Figure 4a,b, the SEI films formed in both BE and BE-FEC-SL/$LiNO_3$ contain LiF (685.2 eV), $Li_xPO_yF_z$ (687.4 eV), and $LiPF_6$ (689.4 eV). In addition, the formation of phosphorus compounds on SEI surface is also confirmed by P 2p spectra in Figure S8, which can be attributed to $LiPF_6$ decomposition and residual $LiPF_6$ salt.[39] However, the peak intensity of LiF formed in BE is much weaker than that in BE-FEC-SL/$LiNO_3$, which is induced by the reduction of FEC additive. Meanwhile, only the LiF peak exists in the F 1s spectrum with an intensive signal after Ar ion sputtering, which confirms more LiF

https://doi.org/10.1021/acsenergylett.1c00365
ACS Energy Lett. 2021, 6, 1839−1848

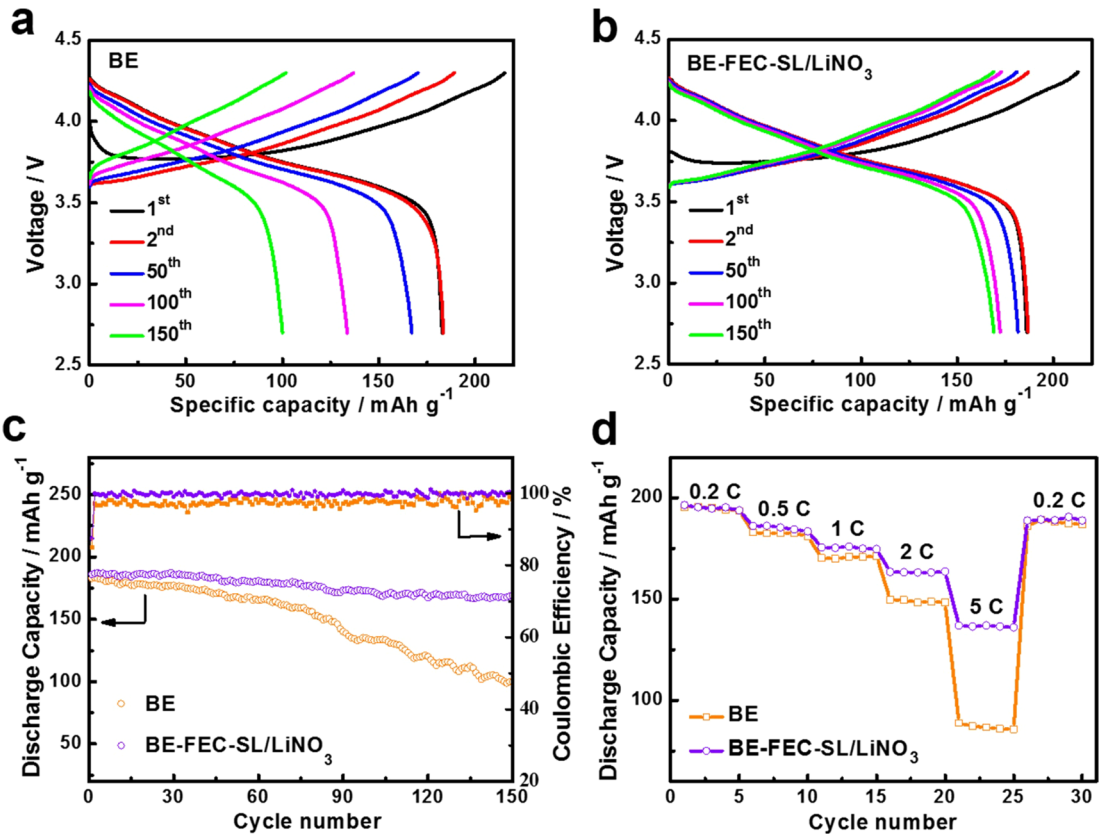

Figure 6. Voltage profiles of NCA||less Li (50 μm) cells with BE (a) and BE-FEC-SL/$LiNO_3$ (b). (c) Long-term cycling of NCA||less Li cells with BE and BE-FEC-SL/$LiNO_3$. The cells were charged and discharged between 2.7 and 4.3 V at a rate of 0.5 C. (d) Rate performance of NCA||less Li cells with BE and BE-FEC-SL/$LiNO_3$.

component is aggregated in the inner SEI. For N 1s spectra, there was no distinct N 1s peak in BE, while several clear peaks including Li_3N at 398.7 eV, LiN_xO_y at 400.4 eV, and $LiNO_2$ at 404.4 eV were captured in BE-FEC-SL/$LiNO_3$.[30,40,41] Moreover, only a clear Li_3N signal can be found after 300 s of sputtering for the SEI formed in BE-FEC-SL/$LiNO_3$. The C and O spectra (Figure S9) and the elemental composition (Figure S10) after sputtering of SEI for different times were also analyzed. In BE, an organic−inorganic SEI with a nonuniform structure is formed, which is consistent with previous studies.[42,43] However, the SEI formed in BE-FEC-SL/$LiNO_3$ has a lower C content but higher F and N content, suggesting fewer organic components but enhanced Li_3N and LiF in the inner SEI. LiF is an electronic insulation and has a high interfacial energy against metallic Li, which can effectively suppress Li dendrites. Besides, Li_3N has ultrahigh Li ion conductivity (10^{-3} S cm^{-1}),[39,44,45] which is effective for the rapid ionic transport. Therefore, a LiF-Li_3N SEI with high lithiophobicity and high ionic conductivity in BE-FEC-SL/$LiNO_3$ enables Li anode to achieve a recorded high plating/striping CE of 99.6%.

The elemental Li, F, N, and O mapping of the SEI on the electrodeposited lithium metal with a Cu foil substrate in BE-FEC-SL/$LiNO_3$ was also characterized by SEM images and energy dispersive spectroscopy (EDS) elemental mapping (Figure S11). As an effective tool to reveal the contrast between different chemical compositions, the backscattered electron image in Figure S11b displays a much darker morphology on the top (metallic Li area due to the lower atomic number) compared with the bottom Cu area. As shown in Figure S11d−g, distinct N, F, O, C signals are found on the surface of lithium metal, which suggest LiF-Li_3N enhanced SEI is formed. Meanwhile, cryogenic scanning TEM electron energy loss spectroscopy (STEM-EELS) with high spatial resolution was further adopted for more chemical information. The high-angle annular dark-field imaging (HAADF, Figure S12) along with the Li K-map, F K-map, N K-map, and O K-map (Figure 4c) were yielded in the SEI region through cryogenic STEM-EELS. The Li K-edge spectrum (Figure S13) displays a major broad peak centered at 61 eV and proves the area is indeed metallic Li. To access a deeper understanding of the SEI structural information, cryogenic high-resolution TEM (cryo-HRTEM) imaging was also captured in Figure 4d, which reveals a compact SEI structure with a thickness around 20 nm. Significant crystalline reflections are found in the image and indicate that a well-passivated SEI is constructed on metallic Li with more inorganic components such as LiF, Li_3N, Li_2O, and Li_2CO_3. These inorganic crystalline particles may be the key contribution for the effective passivation due to their outstanding physicochemical properties, such as their intrinsically low electronic conductivity, relatively high ionic conductivity, and high interfacial energy to suppress Li dendrite growth. The schematic diagram of the SEI formed in BE-FEC-SL/$LiNO_3$ is shown in Figure 4e.

LiF-Li_3N Enhanced SEI Formation Mechanism. Molecular dynamics (MD) simulation was performed to investigate the roles of FEC and SL/$LiNO_3$ additives from the aspect of solvation structure. Figure 5a,c shows the snapshots of simulated BE and BE-FEC-SL/$LiNO_3$ electrolytes. The solvents in the first coordinated shell are depicted by ball

https://doi.org/10.1021/acsenergylett.1c00365
ACS Energy Lett. 2021, 6, 1839−1848

and stick models, while the wireframes stand for the free solvents. The solvation structures of the two electrolytes were compared by the calculated radial distribution functions ($g(r)$, solid lines) and coordination numbers ($n(r)$), dash lines) (Figure 5b,d). The dominant peaks of $g(r)$ appear at 9 Å for Li−P(PF_6^-) in both electrolytes but do not exist in the first solvation shell (within 2.75 Å). It means that the majority of Li^+ and PF_6^- are not in direct contact but exist as a separated ion pair (SSIP-PF_6^-). As shown in Figure 5b, additive-free BE, EC, and DMC molecules have occupied the main parts in the first Li^+ solvation shell with coordination numbers 2.61 and 1.73, forming an organic-rich SEI due to the reduction of carbonate solvents. However, the FEC-SL/$LiNO_3$ additive has significantly altered the solvation structure (Figure 5d). Not only coordination numbers of EC and DMC have been slightly reduced to 2.15 and 1.40, but also SL, NO_3^-, and FEC appear in the primary Li^+ solvation structure with coordination numbers of 0.52, 0.25, and 0.05, respectively. Several typical solvation shells of BE-FEC-SL/$LiNO_3$ with calculated binding energies of Li^+ can be found in Figure S14. Obviously, NO_3^--involved solvation structures have lower binding energies, which means that NO_3^- is more inclined to coordinate with Li^+. Besides, solvated clusters such as contact ion pairs (CIPs, NO_3^- that coordinates to one Li^+) and aggregate clusters (AGGs, NO_3^- that coordinate to two or more Li^+) are formed in the primary Li^+ solvation sheath of BE-FEC-SL/$LiNO_3$. With the existence of NO_3^- solvated clusters and the lowest calculated LUMO of NO_3^- compared to other components (EC, DMC, SL, FEC, and PF_6^-) in BE-FEC-SL/$LiNO_3$ (Figure 5e), NO_3^- will be first reduced on the lithium metal surface, forming the SEI with the Li−N species. Similarly, owning to the lower LUMO than other solvents, FEC species can be preferentially reduced to generate more LiF in the SEI.[40,46] It is worth mentioning that the choice of SL as the carrier solvent for $LiNO_3$ is based on comprehensive considerations. On the one hand, the lowest electrostatic potential (ESP) of SL among all the solvents (SL, EC, DMC, and FEC) means a lowest binding energy of SL with Li^+, as exhibited in Figure 5f, suggesting a stronger affinity of SL with Li^+, which helps to increase the solubility of $LiNO_3$. The binding energies of Li^+ with different solvents are also listed in Figure S15, which is consistent with ESP results. On the other hand, the inherent oxidation stability of SL will not affect the high-voltage stability of the entire electrolyte system.[34]

Electrochemical Performances of NCA||Less Li Full Cells. The BE-FEC-SL/$LiNO_3$ electrolyte was also evaluated in the high-energy $LiNi_{0.80}Co_{0.15}Al_{0.05}O_2$ (NCA)||Li (~50 μm) full cell. The oxidation window of BE-FEC-SL/$LiNO_3$ on the stainless steel electrode was first evaluated by using linear sweep voltammetry (LSV). As shown in Figure S16a, BE-FEC-SL/$LiNO_3$ keeps a high oxidation window up to 4.7 V. Moreover, typical phase transitions for the NCA cathode are shown in the first two cycles of cyclic voltammetry (CV) curves at 3−4.3 V (Figure S16b), proving that a 4.3 V NCA can be used as a cathode in BE-FEC-SL/$LiNO_3$. The electrochemical performance of NCA||Li (50 μm) full cells was evaluated in BE and BE-FEC-SL/$LiNO_3$. The voltage profiles in different cycles for BE and BE-FEC-SL/$LiNO_3$ are shown in Figure 6a,b. NCA||Li cells using the BE-FEC-SL/$LiNO_3$ electrolyte maintains 90.8% capacity retention after 150 cycles with an overall CE up to 99.7%. While the battery without FEC-SL/$LiNO_3$ composite additive only delivered a capacity retention of 54.7% after 150 cycles with an overall CE of 97.4% (Figure 6c). In addition, the rate performance of NCA||Li cells in BE and BE-FEC-SL/$LiNO_3$ was further performed (Figure 6d). The battery with BE-FEC-SL/$LiNO_3$ exhibits considerable discharging capacities of 196, 186, 176, 163, and 137 mAh g^{-1} at 0.2, 0.5, 1, 2, and 5 C, respectively. Especially under a high rate of 5 C, the discharge capacity of BE-FEC-SL/$LiNO_3$ is almost 1.5 times of that obtained in BE (87 mAh g^{-1}). The excellent rate capability may be attributed to the lower interface resistance of the cell with BE-FEC-SL/$LiNO_3$, as revealed by the EIS results for full cells in different electrolytes after 100 cycles (Figure S17).

In summary, the commercial carbonate electrolyte has been proven to have promising application for high-energy NCA/Li metal batteries by simply adding 10 wt % of FEC-SL/$LiNO_3$ composite additives, which promotes the formation an advanced LiF-Li_3N enhanced SEI on the lithium metal surface. Specifically, the extreme low electronic conductivity of LiF is propitious to reduce the SEI thickness, and its high surface energy to the lithium metal can suppress the Li dendrite growth, while the high ionic conductivity of Li_3N is beneficial for the faster Li ion diffusion. As a result, the 1 M $LiPF_6$/EC-DMC-10 wt % (FEC-SL/$LiNO_3$) electrolyte enables the Li metal anode to achieve a CE of 99.6% (0.5 mA cm^{-2}, 0.5 mAh cm^{-2}) for 100 cycles. Moreover, the NCA/Li (50 μm) full cell with the designed electrolyte also achieves an outstanding capacity retention of 90.8% after 150 cycles with a high CE of 99.7%. The synergetic additive strategy reported here, by simply adding 10 wt % of synergetic additive into commercial carbonate electrolytes, enables one of the highest CE for Li plating/stripping as well as the stable cycling for NCA/Li full batteries, which definitely opens an economical choice for the practical application of high-energy-density LMBs.

■ ASSOCIATED CONTENT

Supporting Information

The Supporting Information is available free of charge at https://pubs.acs.org/doi/10.1021/acsenergylett.1c00365.

Morphology changes of lithium anodes during Li plating at different capacities in BE (MP4)

Morphology changes of lithium anodes during Li plating at different capacities in BE-FEC-SL/$LiNO_3$ (MP4)

Electrolytes preparation, electrochemical measurements, materials characterization, computational method, optical morphology images, SEM images, XPS spectra, HAADF image, EELS spectrum, MD simulation results, LSV curves, CV curves, Nyquist plots, galvanostatic profiles, the detailed composition of electrolytes, and summary of the reported CE of Li plating/stripping in different carbonate electrolytes (PDF)

■ AUTHOR INFORMATION

Corresponding Authors

Xiangming He − *Institute of Nuclear and New Energy Technology, Tsinghua University, Beijing 100084, China*; Email: hexm@tsinghua.edu.cn

Chunsheng Wang − *Department of Chemical and Biomolecular Engineering, University of Maryland, College Park, Maryland 20740, United States; Department of Chemistry and Biochemistry, University of Maryland, College Park, Maryland 20740, United States*; orcid.org/0000-0002-8626-6381; Email: cswang@umd.edu

Authors

Nan Piao − *Department of Chemical and Biomolecular Engineering, University of Maryland, College Park, Maryland 20740, United States; Institute of Nuclear and New Energy Technology, Tsinghua University, Beijing 100084, China*

Sufu Liu − *Department of Chemical and Biomolecular Engineering, University of Maryland, College Park, Maryland 20740, United States*

Bao Zhang − *School of Optical and Electronic Information, Huazhong University of Science and Technology, Wuhan 430074, China;* orcid.org/0000-0003-3236-221X

Xiao Ji − *Department of Chemical and Biomolecular Engineering, University of Maryland, College Park, Maryland 20740, United States*

Xiulin Fan − *Department of Chemical and Biomolecular Engineering, University of Maryland, College Park, Maryland 20740, United States*

Li Wang − *Institute of Nuclear and New Energy Technology, Tsinghua University, Beijing 100084, China*

Peng-Fei Wang − *Department of Chemical and Biomolecular Engineering, University of Maryland, College Park, Maryland 20740, United States;* orcid.org/0000-0001-9882-5059

Ting Jin − *Department of Chemical and Biomolecular Engineering, University of Maryland, College Park, Maryland 20740, United States*

Sz-Chian Liou − *Maryland Nanocenter, University of Maryland, College Park, Maryland 20740, United States*

Huicong Yang − *Shenyang National Laboratory for Materials Science, Institute of Metal Research, Chinese Academy of Sciences, Shenyang 110016, China*

Jianjun Jiang − *School of Optical and Electronic Information, Huazhong University of Science and Technology, Wuhan 430074, China;* orcid.org/0000-0001-9178-8988

Kang Xu − *Energy Storage Branch, CCDC Army Research Laboratory, Adelphi, Maryland 20783, United States;* orcid.org/0000-0002-6946-8635

Marshall A. Schroeder − *Energy Storage Branch, CCDC Army Research Laboratory, Adelphi, Maryland 20783, United States*

Complete contact information is available at: https://pubs.acs.org/10.1021/acsenergylett.1c00365

Author Contributions

[∇]N.P., S.-F.L., and B.Z. contributed equally to this work.

Notes

The authors declare no competing financial interest.

■ ACKNOWLEDGMENTS

This work was supported by the Ministry of Science and Technology of China for Sino-U.S. Cooperation (No. 2019YFE0100200). The authors thank Joint Work Plan for Research Projects under the Clean Vehicles Consortium at U.S. and China−Clean Energy Research Center (CERC−CVC2.0, 2016-2020). We acknowledge the University of Maryland supercomputing resources (http://hpcc.umd.edu) made available for conducting DFT computations in this paper. We also thank the Maryland NanoCenter and its AIMLab for support.

■ REFERENCES

(1) Liu, J.; Bao, Z.; Cui, Y.; Dufek, E. J.; Goodenough, J. B.; Khalifah, P.; Li, Q.; Liaw, B. Y.; Liu, P.; Manthiram, A.; Meng, Y. S.; Subramanian, V. R.; Toney, M. F.; Viswanathan, V. V.; Whittingham, M. S.; Xiao, J.; Xu, W.; Yang, J.; Yang, X.-Q.; Zhang, J.-G. Pathways for practical high-energy long-cycling lithium metal batteries. *Nat. Energy* **2019**, *4* (3), 180−186.

(2) Lin, D.; Liu, Y.; Cui, Y. Reviving the lithium metal anode for high-energy batteries. *Nat. Nanotechnol.* **2017**, *12*, 194.

(3) Xu, W.; Wang, J.; Ding, F.; Chen, X.; Nasybulin, E.; Zhang, Y.; Zhang, J.-G. Lithium metal anodes for rechargeable batteries. *Energy Environ. Sci.* **2014**, *7* (2), 513−537.

(4) Albertus, P.; Babinec, S.; Litzelman, S.; Newman, A. Status and challenges in enabling the lithium metal electrode for high-energy and low-cost rechargeable batteries. *Nat. Energy* **2018**, *3* (1), 16−21.

(5) Yue, X.-Y.; Li, X.-L.; Wang, W.-W.; Chen, D.; Qiu, Q.-Q.; Wang, Q.-C.; Wu, X.-J.; Fu, Z.-W.; Shadike, Z.; Yang, X.-Q.; Zhou, Y.-N. Wettable carbon felt framework for high loading Li-metal composite anode. *Nano Energy* **2019**, *60*, 257−266.

(6) Yue, X.-Y.; Wang, W.-W.; Wang, Q.-C.; Meng, J.-K.; Wang, X.-X.; Song, Y.; Fu, Z.-W.; Wu, X.-J.; Zhou, Y.-N. Cuprite-coated Cu foam skeleton host enabling lateral growth of lithium dendrites for advanced Li metal batteries. *Energy Storage Materials* **2019**, *21*, 180−189.

(7) Cheng, X.-B.; Zhang, R.; Zhao, C.-Z.; Zhang, Q. Toward Safe Lithium Metal Anode in Rechargeable Batteries: A Review. *Chem. Rev.* **2017**, *117* (15), 10403−10473.

(8) Suo, L.; Hu, Y.-S.; Li, H.; Armand, M.; Chen, L. A new class of solvent-in-salt electrolyte for high-energy rechargeable metallic lithium batteries. *Nat. Commun.* **2013**, *4*, 1481.

(9) Zheng, J.; Engelhard, M. H.; Mei, D.; Jiao, S.; Polzin, B. J.; Zhang, J.-G.; Xu, W. Electrolyte additive enabled fast charging and stable cycling lithium metal batteries. *Nat. Energy* **2017**, *2*, 17012.

(10) Fan, X.; Chen, L.; Borodin, O.; Ji, X.; Chen, J.; Hou, S.; Deng, T.; Zheng, J.; Yang, C.; Liou, S.-C.; Amine, K.; Xu, K.; Wang, C. Non-flammable electrolyte enables Li-metal batteries with aggressive cathode chemistries. *Nat. Nanotechnol.* **2018**, *13* (8), 715−722.

(11) Wang, J.; Yamada, Y.; Sodeyama, K.; Chiang, C. H.; Tateyama, Y.; Yamada, A. Superconcentrated electrolytes for a high-voltage lithium-ion battery. *Nat. Commun.* **2016**, *7*, 12032.

(12) Zeng, Z.; Murugesan, V.; Han, K. S.; Jiang, X.; Cao, Y.; Xiao, L.; Ai, X.; Yang, H.; Zhang, J.-G.; Sushko, M. L. Non-flammable electrolytes with high salt-to-solvent ratios for Li-ion and Li-metal batteries. *Nat. Energy* **2018**, *3* (8), 674.

(13) Alvarado, J.; Schroeder, M. A.; Pollard, T. P.; Wang, X.; Lee, J. Z.; Zhang, M.; Wynn, T.; Ding, M.; Borodin, O.; Meng, Y. S. Bisalt ether electrolytes: a pathway towards lithium metal batteries with Ni-rich cathodes. *Energy Environ. Sci.* **2019**, *12* (2), 780−794.

(14) Li, N. W.; Yin, Y. X.; Yang, C. P.; Guo, Y. G. An artificial solid electrolyte interphase layer for stable lithium metal anodes. *Adv. Mater.* **2016**, *28* (9), 1853−1858.

(15) Kozen, A. C.; Lin, C.-F.; Pearse, A. J.; Schroeder, M. A.; Han, X.; Hu, L.; Lee, S.-B.; Rubloff, G. W.; Noked, M. Next-generation lithium metal anode engineering via atomic layer deposition. *ACS Nano* **2015**, *9* (6), 5884−5892.

(16) Gao, Y.; Yan, Z.; Gray, J. L.; He, X.; Wang, D.; Chen, T.; Huang, Q.; Li, Y. C.; Wang, H.; Kim, S. H.; Mallouk, T. E.; Wang, D. Polymer-inorganic solid-electrolyte interphase for stable lithium metal batteries under lean electrolyte conditions. *Nat. Mater.* **2019**, *18* (4), 384−389.

(17) Markevich, E.; Salitra, G.; Chesneau, F.; Schmidt, M.; Aurbach, D. Very Stable Lithium Metal Stripping-Plating at a High Rate and High Areal Capacity in Fluoroethylene Carbonate-Based Organic Electrolyte Solution. *ACS Energy Lett.* **2017**, *2* (6), 1321−1326.

(18) Xu, K. Electrolytes and interphases in Li-ion batteries and beyond. *Chem. Rev.* **2014**, *114* (23), 11503−11618.

(19) Zhang, X. Q.; Cheng, X. B.; Chen, X.; Yan, C.; Zhang, Q. Fluoroethylene carbonate additives to render uniform Li deposits in lithium metal batteries. *Adv. Funct. Mater.* **2017**, *27* (10), 1605989.

(20) Wu, J.; Liu, J.; Lu, Z.; Lin, K.; Lyu, Y.-Q.; Li, B.; Ciucci, F.; Kim, J.-K. Non-flammable electrolyte for dendrite-free sodium-sulfur battery. *Energy Storage Materials* **2019**, *23*, 8−16.

(21) Suo, L.; Xue, W.; Gobet, M.; Greenbaum, S. G.; Wang, C.; Chen, Y.; Yang, W.; Li, Y.; Li, J. Fluorine-donating electrolytes enable highly reversible 5-V-class Li metal batteries. *Proc. Natl. Acad. Sci. U. S. A.* **2018**, *115* (6), 1156−1161.
(22) Markevich, E.; Salitra, G.; Aurbach, D. Fluoroethylene carbonate as an important component for the formation of an effective solid electrolyte interphase on anodes and cathodes for advanced Li-ion batteries. *ACS Energy Lett.* **2017**, *2* (6), 1337−1345.
(23) Zhang, L.; Ling, M.; Feng, J.; Mai, L.; Liu, G.; Guo, J. The synergetic interaction between $LiNO_3$ and lithium polysulfides for suppressing shuttle effect of lithium-sulfur batteries. *Energy Storage Materials* **2018**, *11*, 24−29.
(24) Zhang, S. S. Role of $LiNO_3$ in rechargeable lithium/sulfur battery. *Electrochim. Acta* **2012**, *70*, 344−348.
(25) Liang, X.; Wen, Z.; Liu, Y.; Wu, M.; Jin, J.; Zhang, H.; Wu, X. Improved cycling performances of lithium sulfur batteries with $LiNO_3$-modified electrolyte. *J. Power Sources* **2011**, *196* (22), 9839−9843.
(26) Zhang, X.-Q.; Chen, X.; Hou, L.-P.; Li, B.-Q.; Cheng, X.-B.; Huang, J.-Q.; Zhang, Q. Regulating anions in the solvation sheath of lithium ions for stable lithium metal batteries. *ACS Energy Lett.* **2019**, *4* (2), 411−416.
(27) Winter, M.; Barnett, B.; Xu, K. Before Li ion batteries. *Chem. Rev.* **2018**, *118* (23), 11433−11456.
(28) Shi, Q.; Zhong, Y.; Wu, M.; Wang, H.; Wang, H. High-capacity rechargeable batteries based on deeply cyclable lithium metal anodes. *Proc. Natl. Acad. Sci. U. S. A.* **2018**, *115* (22), 5676−5680.
(29) Liu, Y.; Lin, D.; Li, Y.; Chen, G.; Pei, A.; Nix, O.; Li, Y.; Cui, Y. Solubility-mediated sustained release enabling nitrate additive in carbonate electrolytes for stable lithium metal anode. *Nat. Commun.* **2018**, *9* (1), 3656.
(30) Yan, C.; Yao, Y. X.; Chen, X.; Cheng, X. B.; Zhang, X. Q.; Huang, J. Q.; Zhang, Q. Lithium Nitrate Solvation Chemistry in Carbonate Electrolyte Sustains High-Voltage Lithium Metal Batteries. *Angew. Chem.* **2018**, *130* (43), 14251−14255.
(31) Zhang, W.; Wu, Q.; Huang, J.; Fan, L.; Shen, Z.; He, Y.; Feng, Q.; Zhu, G.; Lu, Y. Colossal Granular Lithium Deposits Enabled by the Grain-Coarsening Effect for High-Efficiency Lithium Metal Full Batteries. *Adv. Mater.* **2020**, *32* (24), 2001740.
(32) Li, S.; Zhang, W.; Wu, Q.; Fan, L.; Wang, X.; Wang, X.; Shen, Z.; He, Y.; Lu, Y. Synergistic Dual-Additive Electrolyte Enables Practical Lithium-Metal Batteries. *Angew. Chem., Int. Ed.* **2020**, *59* (35), 14935−14941.
(33) Fu, J.; Ji, X.; Chen, J.; Chen, L.; Fan, X.; Mu, D.; Wang, C. Lithium Nitrate Regulated Sulfone Electrolytes for Lithium Metal Batteries. *Angew. Chem.* **2020**, *132* (49), 22378−22385.
(34) Ren, X.; Chen, S.; Lee, H.; Mei, D.; Engelhard, M. H.; Burton, S. D.; Zhao, W.; Zheng, J.; Li, Q.; Ding, M. S. Localized high-concentration sulfone electrolytes for high-efficiency lithium-metal batteries. *Chem* **2018**, *4* (8), 1877−1892.
(35) Cao, X.; Ren, X.; Zou, L.; Engelhard, M. H.; Huang, W.; Wang, H.; Matthews, B. E.; Lee, H.; Niu, C.; Arey, B. W.; Cui, Y.; Wang, C.; Xiao, J.; Liu, J.; Xu, W.; Zhang, J.-G. Monolithic solid−electrolyte interphases formed in fluorinated orthoformate-based electrolytes minimize Li depletion and pulverization. *Nat. Energy* **2019**, *4* (9), 796−805.
(36) Shin, W.; Zhu, L.; Jiang, H.; Stickle, W. F.; Fang, C.; Liu, C.; Lu, J.; Ji, X. Fluorinated co-solvent promises Li-S batteries under lean-electrolyte conditions. *Mater. Today* **2020**, *40*, 63−71.
(37) Lu, Y.; Tu, Z.; Archer, L. A. Stable lithium electrodeposition in liquid and nanoporous solid electrolytes. *Nat. Mater.* **2014**, *13*, 961.
(38) Tikekar, M. D.; Choudhury, S.; Tu, Z.; Archer, L. A. Design principles for electrolytes and interfaces for stable lithium-metal batteries. *Nat. Energy* **2016**, *1* (9), 16114.
(39) Li, X.; Guo, S.; Deng, H.; Jiang, K.; Qiao, Y.; Ishida, M.; Zhou, H. An ultrafast rechargeable lithium metal battery. *J. Mater. Chem. A* **2018**, *6* (32), 15517−15522.
(40) Xiong, S.; Xie, K.; Diao, Y.; Hong, X. Properties of surface film on lithium anode with $LiNO_3$ as lithium salt in electrolyte solution for lithium−sulfur batteries. *Electrochim. Acta* **2012**, *83*, 78−86.
(41) Li, W.; Yao, H.; Yan, K.; Zheng, G.; Liang, Z.; Chiang, Y.-M.; Cui, Y. The synergetic effect of lithium polysulfide and lithium nitrate to prevent lithium dendrite growth. *Nat. Commun.* **2015**, *6*, 7436.
(42) Wang, A.; Kadam, S.; Li, H.; Shi, S.; Qi, Y. Review on modeling of the anode solid electrolyte interphase (SEI) for lithium-ion batteries. *npj Computational Materials* **2018**, *4* (1), 1−26.
(43) Peled, E.; Golodnitsky, D.; Ardel, G. Advanced Model for Solid Electrolyte Interphase Electrodes in Liquid and Polymer Electrolytes. *J. Electrochem. Soc.* **1997**, *144* (8), L208−L210.
(44) Guo, J.; Wen, Z.; Wu, M.; Jin, J.; Liu, Y. Vinylene carbonate−$LiNO_3$: A hybrid additive in carbonic ester electrolytes for SEI modification on Li metal anode. *Electrochem. Commun.* **2015**, *51*, 59−63.
(45) Xu, H.; Li, Y.; Zhou, A.; Wu, N.; Xin, S.; Li, Z.; Goodenough, J. B. Li_3N-Modified Garnet Electrolyte for All-Solid-State Lithium Metal Batteries Operated at 40 °C. *Nano Lett.* **2018**, *18* (11), 7414−7418.
(46) Hou, T.; Yang, G.; Rajput, N. N.; Self, J.; Park, S.-W.; Nanda, J.; Persson, K. A. The influence of FEC on the solvation structure and reduction reaction of $LiPF_6$/EC electrolytes and its implication for solid electrolyte interphase formation. *Nano Energy* **2019**, *64*, 103881.

https://doi.org/10.1021/acsenergylett.1c00365
ACS Energy Lett. 2021, 6, 1839−1848